Food Hydrocolloids 74 (2018) 159–167

Contents lists available at ScienceDirect

Food Hydrocolloids

journal homepage: www.elsevier.com/locate/foodhyd

Composite and nanocomposite films based on amaranth biopolymers

María Cecilia Condés [a], María Cristina Añón [a], Alain Dufresne [b, c], Adriana Noemi Mauri [a, *]

[a] Centro de Investigación y Desarrollo en Criotecnología de Alimentos (CIDCA) – CCT La Plata-CONICET and Facultad de Ciencias Exactas, Univ. Nacional de La Plata, La Plata, Argentina
[b] Univ. Grenoble Alpes, LGP2, F-38000, Grenoble, France
[c] CNRS, LGP2, F-38000, Grenoble, France

ARTICLE INFO

Article history:
Received 5 June 2017
Received in revised form
12 July 2017
Accepted 13 July 2017
Available online 14 July 2017

Keywords:
Biodegradable films
Amaranth
Protein isolates
Starch nanocrystals
Starch granules

ABSTRACT

The use of amaranth starch granules and nanocrystals as possible reinforcement of amaranth proteins films was analyzed. Starch granules and protein isolates were extracted of amaranth grain, and nanocrystals were prepared by acidic hydrolysis from starch. Films were prepared by casting aqueous dispersions containing amaranth protein isolate (API, 5% w/v), glycerol (1.25% w/v) and different concentrations of starch granules (0–30 wt% relative to API) and nanocrystals (0–12 wt% relative to API). All films were homogeneous, translucent and slightly brownish, with a general visual appearance similar to the control amaranth protein film. While it was possible to prepare films in which the starch granules retain their native structure after being processed, the presence of these particles did not improve the film properties. Only the addition of starch nanocrystals improved their tensile strength and water vapor permeability as well as their water susceptibility, probably due to their nanosize, uniform distribution and the strong interactions that developed with protein matrix.

1. Introduction

Amaranth (*Amaranthus hypochondriacus*) is a naturally resistant ancestral crop that can growth in environments where other cereals or plants cannot, including dry soils, high altitudes, and high temperatures (Omami, Hammes, & Robbertse, 2006). Its flour is produced from the amaranth grain, which is considered to be a pseudocereal. The main biopolymer present in the amaranth grain (approximately 62%) is starch, which occurs as a polygonal shaped granule that has attracted the attention of many researchers due to its small size (1 μm). The protein content of the amaranth grain (approximately 14%) is higher than that of other cereals, thus presenting a balanced composition of essential amino acids and also an important concentration of sulfur ones (Bressani, 1989). The lipid content of the amaranth grain is in the range from 4.8 to 8.1% (Saunders & Becker, 1984).

These biopolymers have been used to prepare edible or biodegradable films, directly from flour, starch and proteins, or mixed with lipids (Tapia-Blácido, Mauri, Menegalli, Sobral, & Añón, 2007; Tapia-Blácido, Sobral, & Menegalli, 2005) that could be used in specific applications — especially those of short service life, such as food packaging or agriculture uses — contributing to resolve the environmental problems caused by the accumulation of nonrenewable and non-biodegradable synthetic materials (mainly derived from petroleum), widely used (Song & Zheng, 2014). In previous works, protein films from native isolates of amaranth protein showed interesting water vapor permeability but poor mechanical properties. These properties could be improved by denaturing proteins partially or totally by thermal or high pressure (HP) treatments prior to film formation. The resulting films showed higher tensile strength, lower water solubility and also lower water vapor permeability (WVP) (only for HP treated films), due to the higher crosslinking of these proteins through hydrogen and disulfides bonds (Condés, Añón, & Mauri, 2013, 2015a).

Currently, the addition of reinforcements and nanoreinforcements into polymer formulations have shown to be one of the most interesting ways to improve the mechanical properties of the resulting materials. Glass fibers, vegetable fibers or cellulose have been added to protein matrices in order to improve their functionality (Beg, Pickering, & Weal, 2005; Liu, Misra, Askeland, Drzal, & Mohanty, 2005; Liu, Mohanty, Askeland, Drzal, & Misra, 2004; Salgado, Schmidt, Molina Ortiz, Mauri, & Laurindo, 2008). Some nanoreinforcements such as clays, nanofibers and nanowhiskers also managed to improve the barrier and mechanical properties of

* Corresponding author. CIDCA, Calle 47 y 116, 1900, La Plata, Argentina.
E-mail address: anmauri@quimica.unlp.edu.ar (A.N. Mauri).

http://dx.doi.org/10.1016/j.foodhyd.2017.07.013
0268-005X/

protein materials (Condés, Añón, Mauri, & Dufresne, 2015b; Echeverría, Eisenberg, & Mauri, 2014; Pereda, Amica, Racz, & Marcovich, 2011).

The characteristics of starch granules such as semicrystalline nature, spherical-polygonal shape and amylose-amylopectin composition, which depend on their botanical origin, as well as its low price and high availability worldwide, leads to wonder whether these particles could be used as reinforcement.

Starch granules have been used in the synthesis of nanocrystals, crystalline platelets that results from the disruption of the semicrystalline structure of starch granules by the acid hydrolysis of amorphous parts. These nanocrystals have been studied as nanoreinforcement for protein matrices (Condés et al, 2015b; González & Alvarez Igarzabal, 2015; Zheng, Ai, Chang, Huang, & Dufresne, 2009). In particular, it was reported that the addition of normal or waxy maize starch nanocrystals improved water vapor permeability, water uptake, surface hydrophobicity and mechanical behavior of amaranth protein films, and also provoked a delay in their weight loss in soil (Condés et al, 2015b).

The aim of this work was to study the possible reinforcement effect of amaranth starch granules or nanocrystals on amaranth protein films. As far as we know, starch granules has not been analyzed in this manner and the very small size of amaranth starch granules make them most interesting; and also the preparation of amaranth nanocrystals has not been reported.

Considering that all the components of these composite and nanocomposite films belong to the same botanical source, they should have a special affinity, which should lead to a better material functionality.

2. Materials and methods

2.1. Plant materials

Seeds of *Amaranthus hypochondriacus* (cultivar 9122) were obtained from Estación Experimental del Instituto Nacional de Tecnología Agropecuaria (INTA), Anguil, La Pampa, Argentina.

2.2. Amaranth flour preparation

Amaranth seeds were ground and screened by 0.092 mm mesh. The resulting flour was defatted with hexane at 25 °C for 5 h (100 g/L suspension) under continuous stirring and filtered. After drying at room temperature, the flour was stored in hermetic containers in a chamber at 4 °C.

2.3. Preparation of amaranth protein isolates

Amaranth protein isolate (API) was prepared according to Martínez and Añón (1996). Briefly, defatted flour was suspended in water (100 g/L) and the pH was adjusted to 11.0 with 2 N NaOH. The suspension was stirred for 60 min at room temperature and then centrifuged for 20 min at 9000 g and 15 °C. The supernatant was adjusted to pH 5.0 with 2 N HCl and then centrifuged at 9000 g for 20 min at 4 °C. The pellet was suspended in water, neutralized with 0.1 N NaOH and freeze-dried. API yield was 8–10 %w/w, and it was stored in hermetic containers in a chamber at 4 °C before use.

2.4. Extraction of amaranth starch granules

Starch extraction was performed according to the method described by Perez, Bahnassey, and Breene (1993) with some modifications. Briefly, the flour sample was immersed in 0.0625 N aqueous NaOH solution and kept at 5 °C for 24 h. Before stepwise filtration through 80 (177 μm), 200 (74 μm) and 270 (53 μm) mesh sieves, the slurry was stirred for about 2 min. Double deionized water was used to wash the slurry until no white starch was washed out. The filtrate was then centrifuged at 4500 g at 10 °C for 20 min (Avanti J-25, Beckman Coulter, California, USA). The supernatant was discarded, and the top yellow protein layer was also removed. The remaining starch layer was resuspended in double deionized water, and neutralized with 2 N HCl. The isolated starch was dried in an oven at 37 °C for 24 h and ground to pass through a mesh 80 (177 μm) and stored in hermetic containers in a chamber at 4 °C until used.

The residual protein content was determined using the technique of microKjeldahl (digestion step) (Allen, 1931) followed by the Berthelot modified colorimetric method (determination of the nitrogen content in the digested) (Tabbaco, Meiattini, Moda, & Tarli, 1979). The protein content of starch was found to be 0.56 ± 0.05 wt %.

2.5. Preparation of starch nanocrystals

Amaranth starch nanocrystals were obtained according to a previously described method (Angellier, Choisnard, Molina-Boisseau, Ozil, & Dufresne, 2004). Briefly, acid hydrolysis of 36.725 g amaranth starch granules was performed in by 250 mL of 3.16 M H_2SO_4 solution, at 40 °C and 100 rpm. The mixture was subjected to an orbital shaking action during 5 days. Subsequently, the ensuing insoluble residue was washed with distilled water and separated by successive centrifugations at 10,000 rpm and 5 °C, until neutrality. The aqueous suspensions of starch nanoparticles were stored at 4 °C after adding several drops of chloroform to inhibit the growth of microorganisms, or freeze-dried according to the requirements of each assay.

2.6. Starch granules and nanocrystals characterization

2.6.1. Amylose content

Amylose content of the starch granules was determined by using the method of Williams, Kuzina, and Hlynka (1970). A starch sample (20 mg) was taken and 10 mL of 0.5 N KOH was added to it. The suspension was thoroughly mixed. The dispersed sample was transferred to a 100 mL volumetric flask and diluted to the mark with distilled water. An aliquot of test starch solution (10 mL) was pipetted into a 50 mL volumetric flask and 5 mL of 0.1 N HCl was added followed by 0.5 mL of iodine reagent. The volume was diluted to 50 mL and the absorbance was measured at 625 nm. The measurement of the amylose content was determined from a standard curve developed using amylose and amylopectin blends. It was performed in duplicate.

2.6.2. Optical microscopy

Optical microscopy examinations using a Leica DMLB (Leica Microsystems, Germany) with a capture camera DC100 (Leica Microscopy Systems Ltd., Switzerland) were carried out on dispersions of starch granules at 1% w/v in water. A magnification of 1000× was used to examine the samples.

2.6.3. Scanning electron microscopy (SEM) and field emission gun scanning electron microscopy (FEG-SEM)

A SEM 505 (Philips, Netherlands) with an accelerating potential of 10 kV was used to examine the shape and surface of starch granules. Starch samples were prepared by applying granules on an aluminum stub using double-sided adhesive tape and coating the starch with gold (Sputter coater, Edwards S150B).

SEM observation performed using a Zeiss DSM982 Gemini with a field emission gun (FEG) was used to examine the shape and surface of starch nanoparticles. The sample was prepared by

depositing 2.5 mL of starch nanocrystal suspension (with concentration of 0.0001% w/v) on a TEM grid.

2.6.4. Particle size determination

The determination of starch nanocrystals size by measuring dynamic light scattering (DLS) was made on a Zetasizer Nano-Zs (Malvern Instruments Ltd., United Kingdom) equipped with a He-Ne laser (633 nm) and a digital correlator (ZEN3600) with a measuring range of 0.6–6000 nm. Measurements at a scattering angle of 173° were performed at room temperature using a polystyrene cell. Nanocrystal dispersions were diluted to 0.05% v/v in milliQ water, thus eliminating the possible turbidity that may exist in the sample at higher concentrations. The sample was illuminated with a laser and the intensity of scattered light produced by the particles fluctuated at a rate that is dependent on particle size. Therefore, using the software provided with the equipment it was possible to obtain the particle size distribution by intensity, determining the average size and the polydispersity index that is the width of the Gaussian bell and reflects the diversity of particle size in the sample. All determinations were performed at least in triplicate.

2.6.5. X-ray diffraction

Amaranth starch granules and nanocrystals were submitted to X-ray radiation using a diffractometer (Philips model PW 1510), with a vertical goniometer operating at Cu Kα radiation wavelength ($\lambda = 0.154$ nm), 40 kV, 30 mA and sampling interval of 0.01°. Scattered radiation was detected in the angular range $2\theta = 5–40°$.

The crystallinity index of the samples was quantitatively estimated following the method of Nara and Komiya (1983) adapted, also called the "two-phase" method. A curve connecting the peaks baseline was plotted on the diffractogram. The area above the curve was assumed to correspond to the crystalline domains, and the lower area to the amorphous part. The ratio of upper area to total area was taken as the crystallinity index.

2.6.6. Differential scanning calorimetry (DSC)

A TA Instrument DSC Q100 V9.8 Build 296 (New Castle, DE, USA) was used to determine the thermal characteristics of starch granules and nanocrystals. Temperature and heat flow calibration of the equipment was carried out according to ASTM standards, using lauric and stearic acid and indium as standards, respectively. For starch granules, hermetically sealed aluminum pans containing 15 mg of starch dispersion (30% w/v in distilled water) were prepared and scanned at 10 °C/min over the range 20–135 °C. For starch nanocrystals, hermetically sealed aluminum pans containing 5 mg of freeze-dried starch nanocrystals were prepared and scanned at 10 °C/min over the range 0–300 °C. Gelatinization and fusion enthalpies (ΔH_{gel} and ΔH_f) and peak temperatures (T_{gel} and T_f) were taken from the corresponding thermograms (Universal Analysis V4.2E, TA Instruments, New Castle, DE, USA). Enthalpy values were expressed as J/g of starch granule or nanocrystal, taking into account the dry weight, determined by perforating the pans and heating overnight at 105 °C.

2.7. Film formation

Films were prepared by casting dispersions of amaranth protein isolate (API, 5% w/v), glycerol (1.25% w/v, Anedra, Argentina) and variable amounts of amaranth starch granules (0, 2.5, 5, 10, 20 and 30 wt% relative to API) or amaranth starch nanocrystals dispersions (0, 3, 6, 9 and 12 wt% relative to API) in distilled water. All dispersions were magnetically stirred for 1 h at room temperature, their pH was adjusted to 10.5 with 2 mol/L NaOH, and they were stirred again for additional 20 min. 10 mL of each film forming dispersion were poured onto polystyrene Petri dishes (64 cm^2) and dried at 40 °C in an oven with air flow and circulation (Yamato, DKN600, USA) for 4:30 h or 3:30 h for films with starch granules or starch nanocrystals, respectively. The dry films were conditioned at 20 °C and 58% relative humidity (RH) in desiccators with saturated solutions of NaBr for 48 h before being peeled from the casting surface for characterization.

2.8. Film characterization

2.8.1. Moisture content (MC)

MC was gravimetrically determined after drying in an oven at 105 °C for 24 h. Small film specimens collected after conditioning, were cut and placed on Petri dishes that were weighed before and after oven drying. MC values were determined in triplicate for each film, and calculated as the percentage of weight loss based on the original weight (ASTM D644-94, 1994).

2.8.2. Film thickness

Film thickness was measured by a digital coating thickness gauge (Check Line DCN-900, USA). Measurements were done at five positions along the rectangular strips for the tensile test, and at the center and at eight positions round the perimeter for the water vapor permeability (WVP) determination. The mechanical properties and WVP were calculated using the average thickness for each film replicate.

2.8.3. Film color

Film color was determined using a Minolta Chroma meter (CR 300, Minolta Chroma Co., Osaka, Japan). A CIELab color scale was used to measure the degree of lightness (L), redness ($+a$) or greenness ($-a$), and yellowness ($+b$) or blueness ($-b$) of the films. The instrument was standardized using a set of three Minolta calibration plates. Films were measured on the surface of the white standard plate with color coordinates of $L = 97.3$, $a = 0.14$ and $b = 1.71$. Total color difference (ΔE) was calculated from:

$$\Delta E = \sqrt{\left(L_{film} - L_{s\ tan\ dard}\right)^2 + \left(a_{film} - a_{s\ tan\ dard}\right)^2 + \left(b_{film} - b_{s\ tan\ dard}\right)^2} \quad (1)$$

Values were expressed as the means of nine measurements on different areas of each film.

2.8.4. Opacity

Each film specimen was cut into a rectangular piece and placed directly in a spectrophotometer test cell, and measurements were

performed using air as the reference. A spectrum for each film was obtained in an UV–Vis spectrophotometer (Beckman DU650, Germany). The opacity of the film (UA/mm) was calculated by dividing the absorbance at 500 nm by the film thickness (mm) (Cao, Fu, & He, 2007). All determinations were performed in triplicate.

2.8.5. Mechanical properties

The tensile strength, Young's modulus and elongation at break of the films were determined following the procedures outlined in the ASTM methods D882-91 (1991), taking an average of six measurements for each film and using at least two films per formulation. The films were cut into 6 mm wide and 80 mm long strips, and mounted between the grips of the texture analyzer TA.XT2i (Stable Micro Systems, Surrey, England). The initial grip separation was set at 50 mm and the crosshead speed at 0.4 mm/s. The tensile strength (force/initial cross-sectional area) and elongation at break were determined directly from the stress–strain curves using Texture Expert V.1.15 software (Stable Micro Systems, Surrey, England), and the Young's modulus was calculated as the slope of the initial linear portion of this curve.

2.8.6. Solubility

Solubility was measured by immersion of film disks (2.0 cm in diameter) in water containing sodium azide, at 25 ± 2 °C for a period of 24 h (Gontard, Guilbert, & Cuq, 1992). The amount of dry matter in the initial and final samples was determined by drying the samples at 105 °C for 24 h. All determinations were performed in triplicate.

2.8.7. Water vapor permeability (WVP)

WVP tests were conducted using ASTM method E96-00 (1996) with some modifications (Gennadios, McHugh, Weller, & Krochta, 1994). Each film sample was sealed over a circular opening of 0.00177 m^2 in a permeation cell that was stored at 25 °C in a desiccator. To maintain a 75% relative humidity (RH) gradient across the film, anhydrous silica (0% RH) was placed inside the cell and a saturated NaCl solution (75% RH) was used in the desiccator. The RH inside the cell was always lower than outside, and water vapor transport was determined from the weight gain of the permeation cell. When steady-state conditions were reached (about 1 h), eight weight measurements were made over 5 h. Changes in the weight of the cell were recorded and plotted as a function of time. The slope of each line was calculated by linear regression and the water vapor transmission rate (WVTR) was calculated from the slope (g/s H_2O) divided by the cell area (m^2). WVP (g/Pa s m) was calculated as:

$$WVP = [(WVTR) \times d] \Big/ \left[P_v^{H_2O} \times (RH_d - RH_c) \times A\right] \quad (2)$$

where P_V^{H2O} = vapor pressure of water at saturation (Pa) at the test temperature (20 °C), RH_d = RH in the desiccator, RH_c = RH in the permeation cell, A = permeation area (m^2), and d = film thickness (m). Each WVP value represents the mean value of at least three sampling units taken from different films.

2.8.8. Water uptake (WU)

The water uptake was determined used samples of rectangular films of 1 cm^2. After weighing to determine the initial weight (m_0), they were placed in a container conditioned at 98% RH using a saturated copper sulfate solution. At specific time intervals, the sample weight (m_t) was determined until an equilibrium value (m_∞) was reached. Three replicates were tested for each sample. The water uptake (WU %) of the sample was calculated as:

$$WU\% = (m_\infty - m_0) \times 100/m_0 \quad (3)$$

2.9. Statistical analysis

Results were expressed as mean ± standard deviation and were analyzed by means of ANOVA. Means were tested with the Fisher's least significant difference test for paired comparison, with a significance level $\alpha = 0.05$.

3. Results and discussion

3.1. Amaranth starch granules and nanocrystals characterization

Amaranth starch granules were analyzed by scanning electronic microscopy (Fig. 1A). These granules showed a polygonal shape with sizes around 1–2.5 μm, in agreement with the observations of Kong, Bao, and Corkem (2009) and Marcone (2001), and had regular granule size. Agglomeration of the granules is observed in the micrograph at low magnification, which could be attributed in part to the drying method used after extraction under laboratory conditions. The size is significantly smaller than that derived from other biological species. These differences could be related with the amyloplast biochemistry and physiology of each plant (Badenhuizen, 1969; Svegmark & Hermansson, 1993).

The total amylose content of amaranth starch was around 4%. This low content makes it to be regarded as “waxy” starch. Fig. 2 shows the X-ray diffraction pattern of these granules. Amaranth starch exhibits reflections at 15.3°, 17.0°, 18.0° and 23.4° corresponding to an ‘A’ type, typical of cereals starches. It had a high

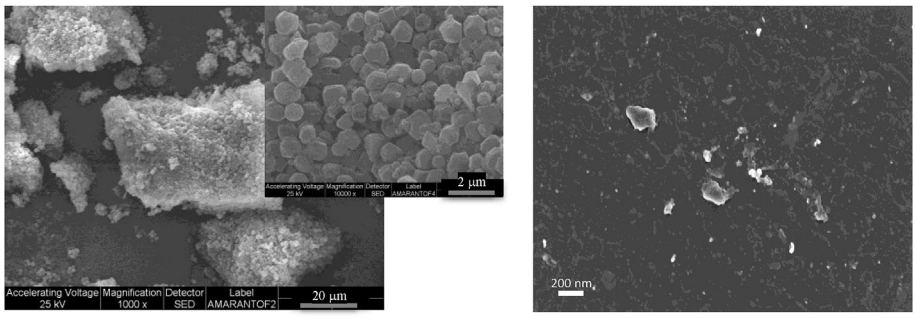

Fig. 1. SEM of amaranth starch granules (A) and FEG-SEM of their nanocrystals (B).

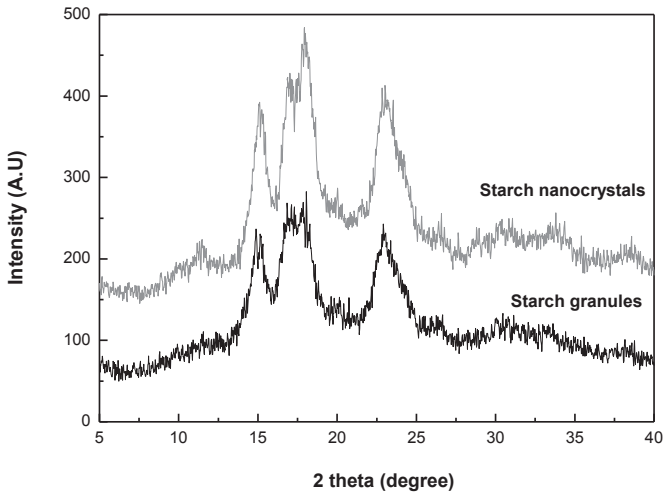

Fig. 2. XRD patterns for amaranth starch granules and nanocrystals.

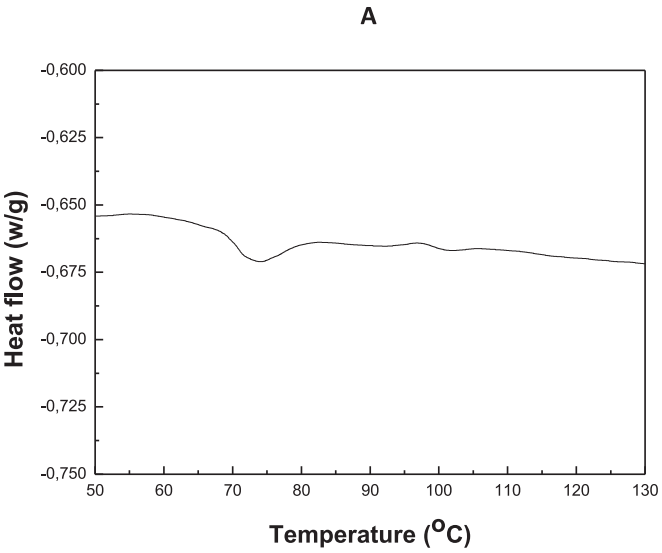

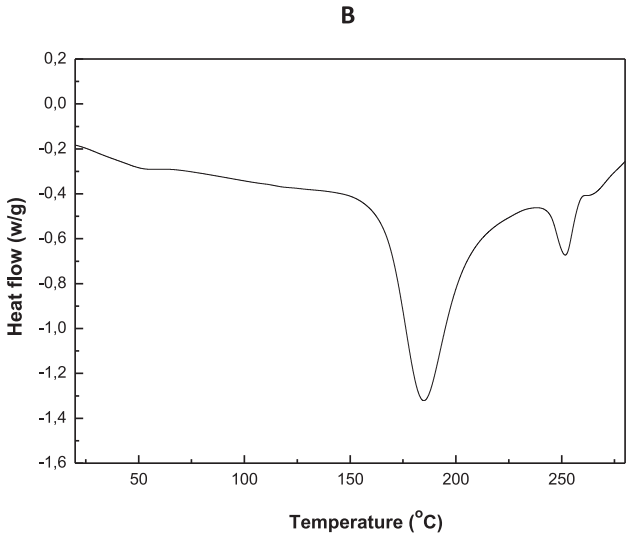

Fig. 3. DSC thermograms for amaranth starch granules (A) and nanocrystals (B).

degree of crystallinity of 34.6% like other waxy starches, because the crystallinity is directly related to the amount of long and short amylopectin chains in the granule (Singh, Singh, Kaur, Sodhi, & Gill, 2003).

Thermogram obtained by DSC for starch dispersion (Fig. 3A) showed an endotherm attributed to starch gelatinization at 73.5 °C (T_{gel}), with a corresponding gelatinization enthalpy (ΔH_{gel}) of 18.4 J/g. These values of T_{gel} and ΔH_{gel} were higher than those found for other sources of starch such as wheat, potato and normal maize and closer to that of waxy maize (Barichello, Yada, Coffin, & Stanley, 1990; Condés et al., 2015b; Liu, Tarn, Lynch, & Skjodt, 2007; Kong et al., 2009; Yoo & Jane, 2002). This might be attributed to the fact that starches with long amylopectin branch chain length, and consequently higher crystallinity, displayed higher structural stability of the granule, resulting in a higher resistance to gelatinization (Barichello et al., 1990). It is worth noting that the process of gelatinization of amaranth starch granules begins at 65 °C. This temperature was considered to set up film drying temperature at 40 °C in order to avoid gelatinization during film formation and ensure that granules remained as such in the final material.

Fig. 1B shows FEG-SEM micrographs obtained for the amaranth starch nanocrystals, which exhibit a platelet-like shape with size near 100 nm -in the nanometric scale- confirming a size modification after acid hydrolysis of the starch granules. The particle size distribution determined with dynamic light scattering showed a single peak of average size equal to 1001 ± 27 nm and a polydispersity of 0.292. It is evident that nanocrystals seen by FEG-SEM formed microaggregates. This trend has been reported by other authors and can be attributed to the large surface area of the platelets and the possible association through hydrogen bonds between hydroxyl groups, which are found in a substantial number

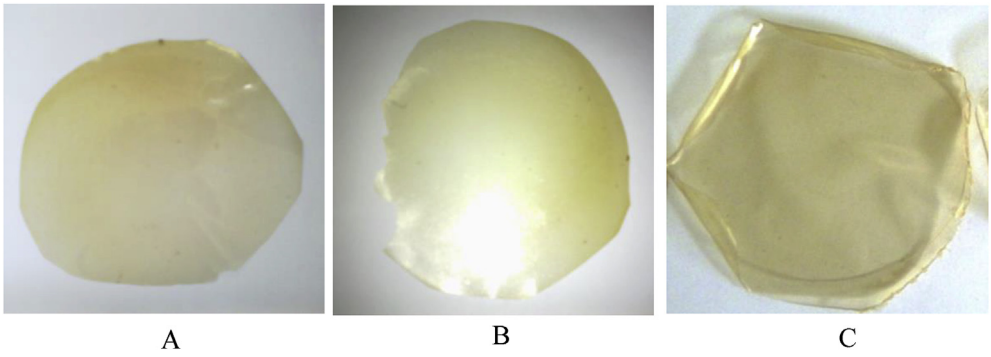

Fig. 4. Neat amaranth protein film (A) and reinforced with 30 wt% of amaranth starch granules (B) or 9 wt% of nanocrystals (C).

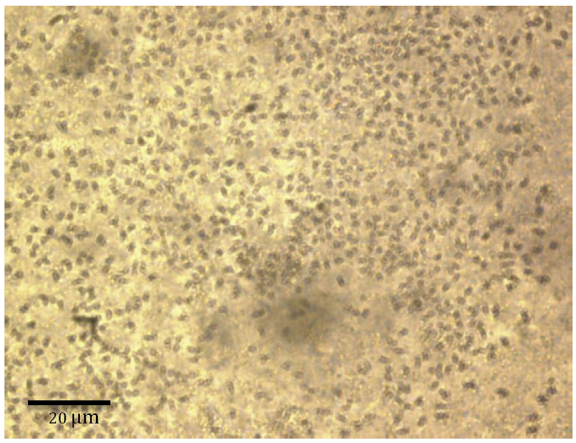

Fig. 5. Optical microscopy of amaranth protein films containing 30 wt% of amaranth starch granules.

for single area of nanocrystals (García, Ribba, Dufresne, Aranguren, & Goyanes, 2011; 2009).

Amaranth starch nanocrystals showed a similar X-ray diffraction pattern to the granules and an unexpected similar crystallinity degree (35.3%) (Fig. 2). It is evident that the hydrolysis conditions studied in this work, previously used by other authors and tuned-ups for corn starch, were not efficient to increase the crystallinity of amaranth nanocrystals. LeCorre, Bras, and Dufresne (2011) also reported lower crystallinity than expected when preparing nanocrystals from waxy starches, which was associated with difficulties in the hydrolysis process in granules with less amorphous areas, and also to the possible hydrolysis of defective amylopectin crystallites by the extension of the process that would induce solubilization of some crystal structure present in the granule.

However, starch nanocrystals showed two endotherms in the DSC thermogram at 181 ± 5 and 252 ± 1 °C, with corresponding enthalpies of 215 ± 14 and 19 ± 1 J/g, respectively (Fig. 3B). These temperature and enthalpy values are higher than those observed for the gelatinization process of starch granules. These two endotherms could be attributed to the fusion of crystals with differences in their thermal stability: a less resistant population that melts first and another comprising more stable crystals melting therefore at higher temperatures (LeCorre, Bras, & Dufresne, 2012; Thielemans, Belgacem, & Dufresne, 2006).

3.2. Films characterization

3.2.1. Appearance

All films prepared by casting with different concentrations of starch granules or nanocrystals were homogeneous, translucent and slightly brownish, with a general visual appearance similar to the control amaranth protein film, as can be seen in Fig. 4.

Fig. 5 shows optical microscopic observation of amaranth protein films containing 30 wt % of amaranth starch granules. Starch granules seemed to remain their native structure into the protein network after being processed by casting. Their shape and size

Table 1
Hunter color values (L, a and b), total color difference (ΔE) and opacity of amaranth protein films with the addition of different contents of amaranth starch granules and nanocrystals.

Starch granules or nanocrystals content % w/w		Hunter-lab color parameters				Opacity (UA/mm)
		L	a	b	ΔE	
Granules	0	83.7 ± 0.8^{a}	−0.6 ± 0.1^{a}	18.2 ± 0.9^{a}	21.4 ± 1.2^{a}	1.8 ± 0.3^{a}
	2.5	83.7 ± 1.0^{a}	−0.5 ± 0.1^{a}	15.3 ± 0.5^{b}	21.2 ± 1.8^{a}	2.4 ± 0.3^{b}
	5	85.1 ± 0.9^{a}	−0.4 ± 0.1^{a}	12.9 ± 1.0^{c}	18.3 ± 1.0^{b}	2.2 ± 0.3^{b}
	10	88.9 ± 0.5^{b}	−0.5 ± 0.1^{a}	11.8 ± 1.0^{c}	17.1 ± 1.1^{b}	2.3 ± 0.9^{b}
	20	84.9 ± 0.9^{a}	−0.3 ± 0.1^{b}	14.2 ± 1.1^{b}	17.7 ± 1.4^{b}	2.6 ± 0.6^{b}
	30	82.8 ± 0.4^{a}	−0.1 ± 0.1^{b}	17.0 ± 0.4^{a}	21.1 ± 0.6^{a}	2.4 ± 0.4^{b}
Nanocrystals	0	83.5 ± 1.4^{a}	−0.1 ± 0.1^{a}	10.2 ± 2.6^{a}	16.2 ± 2.6^{a}	2.6 ± 0.7^{a}
	3	82.7 ± 1.4^{a}	−0.2 ± 0.1^{a}	11.3 ± 2.3^{a}	17.5 ± 2.4^{a}	3.0 ± 0.2^{a}
	6	82.3 ± 0.6^{a}	−0.4 ± 0.1^{a}	12.7 ± 1.0^{a}	18.7 ± 1.1^{a}	2.3 ± 0.3^{a}
	9	81.4 ± 0.8^{a}	−0.2 ± 0.1^{a}	12.0 ± 1.2^{a}	18.9 ± 1.3^{a}	1.2 ± 0.1^{b}
	12	81.6 ± 0.9^{a}	−0.3 ± 0.1^{a}	12.9 ± 1.6^{a}	19.0 ± 1.9^{a}	2.0 ± 0.3^{a}

All values were average ± SD of two values. Reported average values for all parameters within a column with same superscripts (*a*, *b* and *c*) are not significantly different ($P < 0.05$).

Table 2
Water content, water vapor permeability (WVP), water uptake (WU) and water solubility of amaranth protein films with the addition of different contents of amaranth starch granules and nanocrystals.

	Starch granules or nanocrystals content (% w/w)	Water content (%)	WVP $^{*}10^{11}$ (g H_2O/Pa m s)	WU(%)	Solubility (%)
Granules	0	20.1 ± 0.7^{a}	8.1 ± 1.0^{a}	70.9 ± 1.2^{a}	78.6 ± 2.3^{a}
	2.5	19.6 ± 0.9^{a}	8.7 ± 0.2^{a}	80.5 ± 1.9^{b}	79.7 ± 0.8^{a}
	5	19.2 ± 0.3^{a}	8.4 ± 0.7^{a}	80.5 ± 2.5^{b}	80.3 ± 0.9^{a}
	10	19.2 ± 0.7^{a}	8.1 ± 3.0^{a}	81.6 ± 3.4^{b}	80.8 ± 3.0^{a}
	20	19.9 ± 0.3^{a}	9.7 ± 0.5^{a}	80.8 ± 2.1^{b}	91.6 ± 2.2^{b}
	30	18.7 ± 0.3^{a}	9.3 ± 0.7^{a}	80.1 ± 2.6^{b}	79.7 ± 2.5^{a}
Nanocrystals	0	19.1 ± 0.6^{a}	3.0 ± 0.2^{a}	95.0 ± 2.9^{a}	79.6 ± 2.1^{a}
	3	16.4 ± 0.4^{b}	2.6 ± 0.5^{b}	82.6 ± 8.2^{b}	40.8 ± 2.0^{b}
	6	16.5 ± 0.3^{b}	2.2 ± 0.1^{b}	70.8 ± 7.0^{c}	37.4 ± 0.3^{b}
	9	16.1 ± 0.4^{b}	2.1 ± 0.1^{b}	65.4 ± 5.2^{c}	38.5 ± 1.9^{b}
	12	17.0 ± 0.4^{b}	2.3 ± 0.2^{b}	72.0 ± 1.4^{c}	41.6 ± 1.1^{b}

All values were average ± SD of two values. Reported average values for all parameters within a column with same superscripts (*a*, *b* and *c*) are not significantly different ($P < 0.05$).

appeared to be intact. The small granule size and the microscope resolution hindered the view of starch Maltese cross that would confirm that granules retained their semi-crystalline state since the gelatinization did not happen, as it was possible to observe with larger granules of different botanical origin (Condés et al., 2013).

The addition of starch granules or nanocrystals to the protein matrix did not modify the thickness of protein films (≅ 70 μm), which would indicate a good association between the protein matrix and the starch reinforcement probably due to the same botanical origin.

Color parameters and opacity of the studied films are shown in Table 1. The addition of 5, 10 and 20 wt% of starch granules decreased the total color difference (ΔE), which was mainly due to the contribution given by the change in each parameter simultaneously (a decrease in *b* and an increase in *a* and *L*). Nevertheless, the opacity increased significantly with the addition of starch

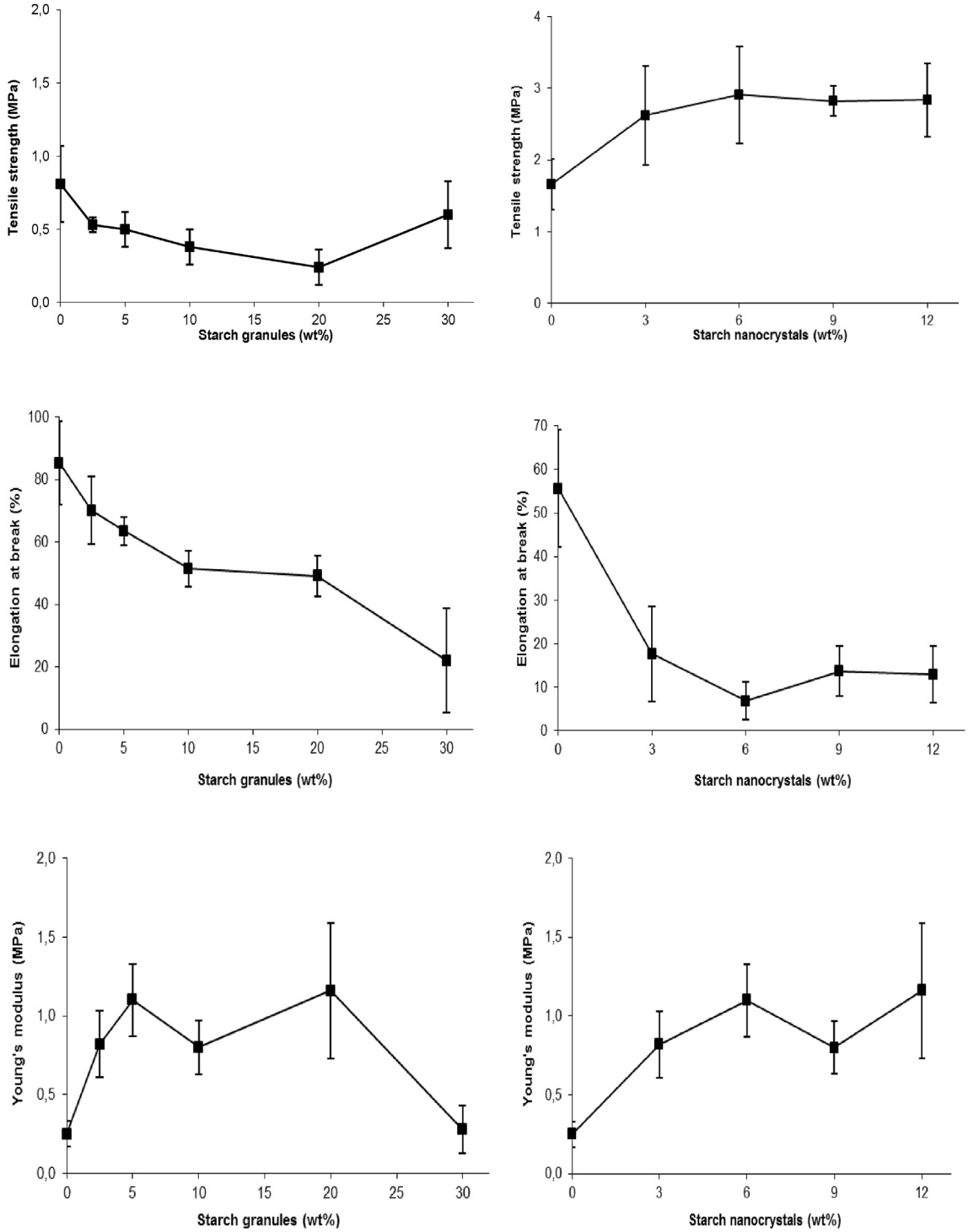

Fig. 6. Mechanical properties: tensile strength, elongation at break and Young's modulus of amaranth protein films with the addition of different contents of starch granules and nanocrystals.

granules in the protein matrix. Granules might scatter light, reducing transparency and increasing opacity of films. However, with the addition of nanocrystals no significant differences neither in color parameters (*a, b, L*, and *ΔE*) nor in opacity were observed, with the exception of films with 9 wt% of nanocrystals, which showed a lower opacity. The fact that the presence of nanocrystals did not affect the degree of compaction of the material, neither its color nor opacity could be attributed to a good dispersion of the nanoreinforcement in the protein matrix due to the good chemical affinity between both components. Several authors suggested that the absence of reduction in the amount of light being transmitted through nanocomposite films is an indication that the nanoreinforcement is fully exfoliated. As a result there should not be a large difference in the amount of light being transmitted through the nanocomposite films compared to the pure matrix (Petersson & Oksman, 2006).

3.2.2. Water susceptibility

Table 2 reports the water susceptibility data for films. Water content, water solubility, water vapor permeability (WVP) and water uptake (WU) for films with different concentrations of starch granules or nanocrystals are shown there. The addition of starch granules to the protein matrix did not modify any of these properties, with the exception of the water uptake that was increased regardless the granule concentration. This increase could be attributed to the ability of the starch granules to absorb water, but probably another factor should be affecting this property because the observed increase was not progressive with concentration. It is evident that the presence of granules did not affect significantly neither the crosslinking of the protein matrix nor its hydrophilic nature, considering that the protein network would be probably formed by native globular proteins (Condés, Speroni, Mauri, & Añón, 2012).

However, the addition of starch nanocrystals decreased the water susceptibility of protein films. All the studied nanocomposites films showed a significant decrease in water content, WVP and solubility regardless the nanocrystal concentration. In particular, the film solubility decreased by half (from 80 to 40%). It is also observed that the water uptake decrease became more significant from 6% of added nanocrystals. García, Ribba, Dufresne, Aranguren, and Goyanes (2009) also reported a decrease in WVP of 40% with the addition of 2.5 wt% cassava starch nanocrystals to a cassava starch matrix and ascribed it to the formation of a tortuous path for water molecules through the film due to the platelet structure of nanocrystals (Kristo & Biliaderis, 2007; LeCorre, Bras, & Dufresne, 2010). Here it is evident that presence of nanocrystals affected the protein crosslinking. Protein/nanocrystal interactions, mainly through hydrogen bonds formation, would leave less hydrophilic groups exposed to the surrounding medium. These interactions also should probably modify protein conformation, making the protein network more hydrophobic. These interactions seem to be resistant against water, as was observed in solubility tests.

3.2.3. Mechanical properties

Fig. 6 shows the mechanical properties for protein films upon addition of increasing amounts of starch granules or nanocrystals.

The addition of starch granules to protein films increased the Young's modulus, but decreased their elongation and tensile strength. The presence of disruptions at microscopic level -not observed with the naked eye- due to non-homogeneous distribution of the granules, or poor interactions between granules and proteins could act as stress concentrators that could anticipate the film's break despite their higher modulus.

It was expected that the small size of amaranth granules would induce a higher reinforcing effect. However, the starch granules agglomeration effect observed in Fig. 1, may contribute in part to the non-homogeneous distribution within the matrix, which avoid this size effect.

The addition of starch nanocrystals to protein films produced an interesting reinforcement effect. The Young's modulus and tensile strength increased with the nanocrystal addition while the elongation at break decreased. This mechanical behavior could be attributed to the good dispersion and the good affinity between starch nanocrystals and proteins that result in strong interactions. This affinity was also suggested in the previous section, when analyzing the films thickness, color, opacity, and water susceptibility. Several authors have attributed starch nanocrystals reinforcement effect to their uniform distribution into polymeric films, which can be achieved due to their small size and the strong interactions that can be formed between nanocrystals and hydrophilic matrices, such as soy protein isolate, polyvinyl alcohol or starch (Chen, Cao, Chang, & Huneault, 2008; Viguié, Molina-Boisseau, & Dufresne, 2007; Zheng et al., 2009).

4. Conclusions

The use of amaranth starch granules and nanocrystals as reinforcement of amaranth proteins films was analyzed. While it was possible to obtain homogenous films with different concentrations of both micro and nanoparticles, only the addition of starch nanocrystals could cause a significant reinforcing effect of the protein matrix. This effect was evidenced by the improved mechanical and barrier properties of the nanocomposites and could be attributed to the strong interactions that can be formed between amaranth nanocrystals and protein matrix.

Initial amaranth starch granules agglomeration could be affecting their dispersion in protein film preventing the material from achieving the expected reinforcing effect due to the small size of the granules.

Acknowledgments

The authors gratefully acknowledge the CNRS (France) and CONICET (Argentina) Cooperation Project, and National Agency of Scientific and Technological Support of Argentina (SECyT, PICT 2010-1837 and 2013-2124) for financial support.

LGP2 is part of the LabEx Tec 21 (Investissements d'Avenir - grant agreement n°ANR-11-LABX-0030) and of the PolyNat Carnot Institut (Investissements d'Avenir - grant agreement n°ANR-11-CARN-030-01).

References

Allen, W. F. (1931). A micro-Kjeldahl method for nitrogen determination. *Journal of the American Oil Chemists' Society, 8*(10), 391–397.

Angellier, H., Choisnard, L., Molina-Boisseau, S., Ozil, P., & Dufresne, A. (2004). Optimization of the preparation of aqueous suspensions of waxy maize starch nanocrystals using a response surface methodology. *Biomacromolecules, 5*, 1545–1551.

ASTM D644-94. (1994). Standard test methods for moisture content of paper and paperboard by oven drying. In *Annual book of ASTM standards*. Philadelphia, PA: USA.

ASTM E96-00. (1996). Standard test methods for water vapor transmission of materials. In *Annual book of ASTM*. Philadelphia, PA: USA.

Badenhuizen, N. P. (1969). *The biogenesis of starch granules in higher plants*. New York: Appeleton Crofts.

Barichello, V., Yada, R. Y., Coffin, R. H., & Stanley, D. W. (1990). Low temperature sweetening in susceptible and resistant potatoes: Starch structure and composition. *Journal of Food Science, 54*, 1054–1059.

Beg, M. D. H., Pickering, K. L., & Weal, S. J. (2005). Corn gluten meal as a biodegradable matrix material in wood fibre reinforced composites. *Materials Science and Engineering, 412*, 7–11.

Bressani, R. (1989). The proteins of grain amaranth. *Food Review International, 5*, 13–38.

Cao, N., Fu, Y., & He, J. (2007). Preparation and physical properties of soy protein isolate and gelatin composite films. *Food Hydrocolloids, 21*, 1153–1162.
Chen, Y., Cao, X., Chang, P. R., & Huneault, M. A. (2008). Comparative study on the films of poly(vinyl alcohol)/pea starch nanocrystals and poly(vinyl alcohol)/native pea starch. *Carbohydrate Polymers, 73*, 8–17.
Condés, M. C., Añón, M. C., & Mauri, A. N. (2013). Amaranth protein films from thermally treated proteins. *Journal of Food Engineering, 119*(3), 573–579.
Condés, M. C., Añón, M. C., & Mauri, A. N. (2015a). Amaranth protein films from high pressure treated proteins. *Journal of Food Engineering, 166*, 38–44.
Condés, M. C., Añón, M. C., Mauri, A. N., & Dufresne, A. (2015b). Amaranth protein films reinforced with maize starch nanocrystals. *Food Hydrocolloids, 47*, 146–157.
Condés, M. C., Speroni, F., Mauri, A. N., & Añón, M. C. (2012). Physicochemical and structural properties of amaranth protein isolates treated with high pressure. *Innovative Food Science & Emerging Technologies, 14*, 11–17.
Echeverría, I., Eisenberg, P., & Mauri, A. N. (2014). Nanocomposites films based on soy proteins and montmorillonite processed by casting. *Journal of Membrane Science, 449*(1), 15–26.
García, N., Ribba, L., Dufresne, A., Aranguren, M. I., & Goyanes, S. (2009). Physico-mechanical properties of biodegradable starch nanocomposites. *Macromolecular Materials Engineering, 294*, 169–177.
García, N. L., Ribba, L., Dufresne, A., Aranguren, M., & Goyanes, S. (2011). Effect of glycerol on the morphology of nanocomposites made from thermoplastic starch and starch nanocrystals. *Carbohydrate Polymers, 84*, 203–210.
Gennadios, A., McHugh, T. H., Weller, C. L., & Krochta, J. M. (1994). Edible coatings and film based on proteins. In J. M. Krochta, E. A. Baldwin, & M. Nisperos-Carriedo (Eds.), *Edible coatings and films to improve food quality* (pp. 201–278). Lancaster: Technomic Publishing Co., Inc.
Gontard, N., Guilbert, S., & Cuq, J. (1992). Edible wheat gluten films: Influence of the main process variables on films properties using response surface methodology. *Journal of Food Science, 57*, 190–195.
González, A., & Alvarez Igarzabal, C. (2015). Nanocrystal-reinforced soy protein films and their application as active packaging. *Food Hydrocolloids, 43*, 777–784.
Kong, X., Bao, J., & Corkem, H. (2009). Physical properties of *Amaranthus* starch. *Food Chemistry, 113*(2), 371–376.
Kristo, E., & Biliaderis, C. G. (2007). Physical properties of starch nanocrystal-reinforced pullulan films. *Carbohydrate Polymers, 68*, 146–158.
LeCorre, D., Bras, J., & Dufresne, A. (2010). Starch nanoparticles: A review. *Biomacromolecules, 11*, 1139–1153.
LeCorre, D., Bras, J., & Dufresne, A. (2011). Influence of botanic origin and amylose content on the morphology of starch nanocrystals. *Journal of Nanoparticle Research, 13*, 7193–7208.
LeCorre, D., Bras, J., & Dufresne, A. (2012). Influence of native starch's properties on starch nanocrystals thermal properties. *Carbohydrate Polymers, 87*, 658–666.
Liu, W., Misra, M., Askeland, P., Drzal, L. T., & Mohanty, A. K. (2005). 'Green' composites from soy based plastic and pineapple leaf fiber: Fabrication and properties evaluation. *Polymer, 46*(8), 2710–2721.
Liu, W., Mohanty, A. K., Askeland, P., Drzal, L. T., & Misra, M. (2004). Influence of fiber surface treatment on properties of Indian grass fiber reinforced soy protein based biocomposites. *Polymer, 45*(22), 7589–7596.
Liu, Q., Tarn, R., Lynch, D., & Skjodt, N. M. (2007). Physicochemical properties of dry matter and starch from potatoes grown in Canada. *Food Chemistry, 105*, 897–907.
Marcone, M. F. (2001). Starch properties of *Amaranthus pumilus* (seabeach amaranth): A threatened plant species with potential benefits for the breeding/amelioration of present *Amaranthus* cultivars. *Food Chemistry, 73*, 61–66.
Martínez, E. N., & Añón, M. C. (1996). Composition and structural characterization of amaranth protein isolates. *Journal of Agricultural Food Chemistry, 44*, 2523–2530.
Nara, S., & Komiya, T. (1983). Studies on the relationship between water-satured state and crystallinity by the diffraction method for moistened potato starch. *Starch/Starke, 35*(12), 407–410.
Omami, E. N., Hammes, P. S., & Robbertse, P. J. (2006). Differences in salinity tolerance for growth and water-use efficiency on some amaranth genotypes. *New Zealand Journal of Crop and Horticultural Science, 34*, 11–22.
Pereda, M., Amica, G., Racz, I., & Marcovich, N. E. (2011). Structure and properties of nanocomposite films based on sodium caseinate and nanocellulose fibers. *Journal of Food Engineering, 103*(1), 76–83.
Perez, E., Bahnassey, Y. A., & Breene, W. M. (1993). A simple laboratory scale method for isolation of amaranth starch. *Starch, 45*(6), 211–214.
Petersson, L., & Oksman, K. (2006). Biopolymer based nanocomposites: Comparing layered silicates and microcrystalline cellulose as nanoreinforcement. *Composites Science and Technology, 66*, 2187–2196.
Salgado, P. R., Schmidt, V. C., Molina Ortiz, S. E., Mauri, A. N., & Laurindo, J. B. (2008). Biodegradable foams based on cassava starch, sunflower proteins and cellulose fibers obtained by a baking process. *Journal of Food Engineering, 85*, 435–443.
Saunders, R., & Becker, R. (1984). Amaranthus: A potential food and feed resource. In Y. Pomeranz (Ed.), *Advances in cereal science and technology* (pp. 357–397). St. Paul: American Association of Cereal Chemists.
Singh, N., Singh, J., Kaur, L., Sodhi, N. S., & Gill, B. S. (2003). Morphological, thermal and rheological properties of starches from different botanical sources. *Food Chemistry, 81*, 219–231.
Song, Y., & Zheng, Q. (2014). Ecomaterials based on food proteins and polysaccharides. *Polymer Reviews, 54*, 514–571.
Svegmark, K., & Hermansson, A. M. (1993). Microstructure and rheological properties of composites of potato starch granules and amylose: A comparison of observed and predicted structure. *Food Structure, 12*, 181–193.
Tabbaco, A., Meiattini, F., Moda, E., & Tarli, P. (1979). Simplified enzymic colorimetric serum urea nitrogen determination. *Clinical Chemistry, 25*, 336–337.
Tapia-Blácido, D., Mauri, A. N., Menegalli, F. C., Sobral, P. J. A., & Añón, M. C. (2007). Contribution of the starch, protein, and lipid fractions to the physical, thermal, and structural properties of amaranth (*Amaranthus caudatus*) flour films. *Journal of Food Science, 72*(5), 293–300.
Tapia-Blácido, D., Sobral, P. J. A., & Menegalli, F. C. (2005). Development and characterization of biofilms based on amaranth flour (*Amaranthus caudatus*). *Journal of Food Engineering, 67*(1–2), 215–223.
Thielemans, W., Belgacem, M. N., & Dufresne, A. (2006). Starch nanocrystals with large chain surface modifications. *Langmuir, 22*(10), 4804–4810.
Viguié, J., Molina-Boisseau, S., & Dufresne, A. (2007). Processing and characterisation of waxy maize starch films plasticized by sorbitol and reinforced with starch nanocrystals. *Macromolecular Bioscience, 7*(11), 1206–1216.
Williams, P. C., Kuzina, F. D., & Hlynka, I. (1970). A rapid calorimetric procedure for estimating the amylose content of starches and flours. *Cereal Chemistry, 47*, 411–420.
Yoo, S., & Jane, J. (2002). Structural and physical characteristics of waxy and other wheat starches. *Carbohydrate Polymers, 49*, 297–305.
Zheng, H., Ai, F., Chang, P. R., Huang, J., & Dufresne, A. (2009). Structure and properties of starch nanocrystal-reinforced soy protein plastics. *Polymer Composites, 30*, 474–480.